Geometry of intensive scalar mixing events in turbulence

Dan Kushnir,[1] Jörg Schumacher,[2] and Achi Brandt[1]

[1]*Department of Computer Science and Applied Mathematics,*
The Weizmann Institute of Science, 76100 Rehovot, Israel

[2]*Department of Mechanical Engineering,*
Technische Universität Ilmenau, D-98684 Ilmenau, Germany

(Dated: January 11, 2006)

Abstract

Maxima of the scalar dissipation rate in turbulence appear in form of sheets and correspond with potentially most intensive scalar mixing events. Their cross-section thickness determines a local diffusion scale. The distribution of this scale is analysed with a fast multiscale clustering algorithm which is applied to very high-resolution simulation data. The thickness is found to be distributed across the whole viscous-convective Batchelor range and beyond. The dissipation maxima vary as the Kolmogorov (Batchelor) scale with respect to the Reynolds (Schmidt) number keeping the other parameter fixed in each case. The distribution of the thickness scales is traced back to the quasi-Gaussian distribution of the contractive short-time Lyapunov exponent of the flow.

PACS numbers: 47.54.-r, 02.70.-c, 07.05.Pj

Introduction. The mixing of a scalar field $\theta(\mathbf{x}, t)$ in a fluid depends strongly on the ratio of the kinematic fluid viscosity ν to the scalar diffusivity κ which is captured by the Schmidt number $Sc = \nu/\kappa$. The case of $Sc > 1$ appears in numerous systems, e.g. for the mixing of phytoplankton or salinity by large scale ocean flows, the turbulent combustion of fuel and oxygen, the low-speed mixing in small devices [1], or the transport of reactive tracers in the stratosphere [2]. In turbulence, this case is known as the Batchelor regime [3] and established between the Kolmogorov scale of the flow, $\eta = (\nu^3/\langle\epsilon\rangle)^{1/4}$, and the Batchelor scale, $\eta_B = \eta/\sqrt{Sc}$, with $\langle\epsilon\rangle$ being the statistical mean of the energy dissipation rate of the flow. Then the scales across which the most intensive mixing events take place, and therefore the strongest scalar gradients exist, are mainly smaller than the Kolmogorov scale. They are important since they determine global mixing efficiency measures [4] or enter directly small-scale parametrizations of mixing, as for the flamelet approach to non-premixed combustion [5]. Our Letter focusses therefore on the size distribution and generation mechanisms of exactly these fine scales for the scalar dissipation rate which probes the magnitude of scalar gradients,

$$\epsilon_\theta(\mathbf{x}, t) = \kappa |\nabla\theta(\mathbf{x}, t)|^2 \,. \tag{1}$$

Tiny gradient scales in the Batchelor regime arise from the competition of two permanently varying processes. On one hand, the scales will be determined by the statistics of the local expansion and contraction rates in the turbulent fluid which can be calculated as the real parts of the eigenvalues of the local velocity gradient tensor $\partial_i u_j$. They are usually denoted by $\alpha(t) \geq \beta(t) \geq \gamma(t)$ and describe a continued stretch-twist-fold motion of the local smooth flow [6]. On the other hand, the scale distribution will be affected by molecular diffusion that causes a diminishing of existing steep gradients as well as the completion of their formation by reconnection [7].

Experimental studies on the geometry of scalar dissipation fields are challenging and only a few exist [8, 9]. Only recently, all gradient components of turbulent fields could be measured directly in moderate Reynolds number flows [10]. The growing computing power made it possible to study high-Sc mixing dynamics in its full complexity within direct numerical simulations (DNS) which discretize the equations of motion on huge grids of up to 10^9 mesh points [11]. Figure 1 shows a two-dimensional (2D) slice cut through such a high-resolution DNS snapshot of $\epsilon_\theta(\mathbf{x}, t)$ in a logarithmic gray color coding. The points that

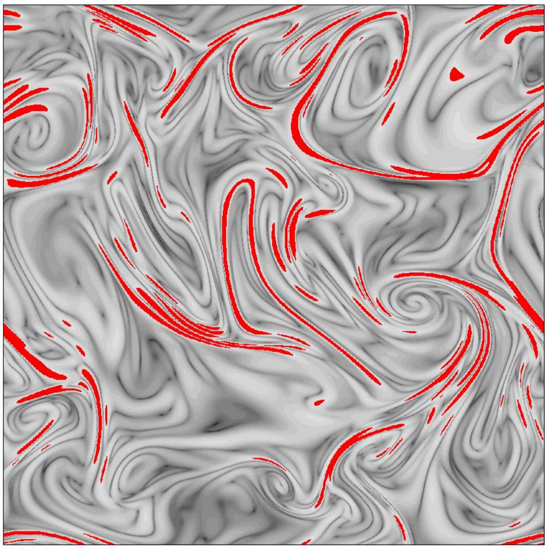

FIG. 1: (color online) Contour plot of a two-dimensional slice cut through the instantaneous three-dimensional scalar dissipation rate field, $\epsilon_\theta(\mathbf{x}, t)$, in units of the mean scalar dissipation rate $\langle\epsilon_\theta\rangle$. The level set L_C for $C = 4$ (see Eq. (2)) is replotted in red. Data are from a pseudospectral simulation of the advection-diffusion equation for the passive scalar in combination with Navier-Stokes equations for a statistically stationary, homogeneous isotropic flow at a resolution of $N^3 = 1024^3$ grid points in a periodic box of volume $V = (2\pi)^3$ [11]. The passive scalar fluctuations are sustained by a linear mean scalar gradient. The Schmidt number is $Sc = 32$ and the Taylor microscale Reynolds number is $R_\lambda = \sqrt{15/(\nu\langle\epsilon\rangle)}\,\langle u_x^2\rangle = 24$ with $\langle\epsilon\rangle$ being the mean energy dissipation rate. The smallest scale in the mixing problem is the Batchelor scale η_B which is resolved with 2 grid cells resulting in a spectral resolution criterion of $k_{max}\eta_B \approx 6$ with $k_{max} = \sqrt{2}N/3$. This resolution is larger by a factor of 4 then the resolution usually adopted.

form the level set of largest amplitudes

$$L_C = \{\mathbf{x} \;:\; \epsilon_\theta(\mathbf{x}, t) \geq C\langle\epsilon_\theta\rangle\}\,, \tag{2}$$

are redrawn in red. The resulting filaments are cross-sections of thin sheets in which the maxima of scalar dissipation are found in the three-dimensional volume [11]. A closer inspection of Fig. 1 unravels various length and thickness scales of the filaments. The filaments are curved and tightly clustered in certain locations thus posing a challenge of separating each curved filament and computing its accurate local width.

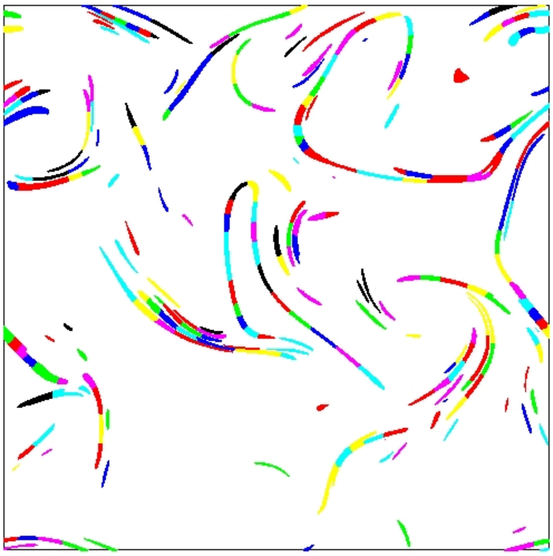

FIG. 2: (color online) Reconstruction of the red colored filaments as shown in Fig. 1 by means of the fast multiscale clustering algorithm. Long filaments are composed of several subfilaments that are colored differently for a better visibilty.

In the following, we want to study the geometry of exactly such intensive dissipation filaments as shown in Fig. 1. We want to answer the following questions: i) How is the filament thickness distributed in relation to the Kolmogorov scale η and to the Batchelor scale η_B? ii) How is the thickness distribution depending on the Reynolds and Schmidt numbers? iii) In which way is their formation determined by the statistics of the expansion and contraction rates of the flow? We will base the analysis on data from high-resolution direct numerical simulations in a periodic cube. Since our focus is on a structural analysis of extreme mixing events, in the present simulations more rigorous resolution requirements have to be applied than is usual case. Three data sets with two different Reynolds and Schmidt numbers, respectively, are taken. For each data set, we analyze at least 12 different plane cuts through the three-dimensional snapshots and consider two statistically independent snapshots which are separated by at least one large scale eddy turnover time.

Multiscale algorithm. Figure 1 demonstrates that the local geometric analysis requires a disentanglement of the filaments that all together form the set L_C. This is done here by a recently developed fast multiscale clustering algorithm [12], which is based on the Segmentation by Weighted Aggregation (SWA) algorithm [13], motivated by Algebraic Multigrid (AMG) [14]. The algorithm assigns data points into clusters in a time linear to the number of points. It starts at the finest resolution level ($s = 0$), the grid spacing. All points $\mathbf{x}_i \in L_C$ are gathered in a so-called proximity graph that contains their location and their connectivity to other points of L_C as quantified by the inter-point weights $w_{ij} = \exp(-b|\mathbf{x}_i - \mathbf{x}_j|)$ where parameter $b \approx 3$. The exponential weight probes the nearest neighbors of each point only. The algorithm gathers points into aggregates of points and aggregates into coarser aggregates successively. It detects a filament as a salient cluster. Saliency is measured by dividing the sum of inter-point weights between points that belong to the cluster and those that do not, with the sum of weights between the points that belong to the cluster.

The algorithm is also used as a tool to accurately measure the filaments widths in the following way. Since the information about proximity is kept as one moves from finer to coarser resolution level, one can perform a fast recursive computation of the covariance matrix $C_{ij}(k, s)$ of the grid points belonging to an aggregate k at a resolution level $s > 0$. The principal component analysis (PCA) of $C_{ij}(k, s)$ results in the set of eigenvectors $\{\mathbf{v}_1(k, s), \mathbf{v}_2(k, s)\}$ and the corresponding eigenvalues $\delta_1(k, s) \geq \delta_2(k, s)$ for the two-dimensional case. The eigenvalues characterize the length and width of the point clusters. Strongly curved filaments remain problematic. Applying a PCA to a whole curved filament will clearly yield a wrong thickness value. Hence, we use the multiscale decomposition of the filaments (aggregates) into convex sub-filaments (finer scale sub-aggregates), which is done by applying a local convexity criterion along the filament. A sub-filament is called *convex* if all points can be connected with links inside the set. Figure 2 shows the reconstruction of the filaments from Fig. 1 and their division into sub-filaments. The local dissipation filament thickness, l_d, is then given by nothing else but the smaller eigenvalue δ_2 following from a PCA of each sub-filament.

Distribution of local dissipation filament thickness. Figure 3 shows the probability density functions (PDF) of the local filament thickness l_d for different (Sc, R_λ). The distribution will depend on the cut-off level C, but the physical picture will not change since C is fixed with respect to the (physically relevant) mean scalar dissipation rate throughout the analysis. Local thickness values within the whole Batchelor range between η_B and η and beyond are found, indicating that dissipation maxima are also related to scalar gradients across inertial range scales. The 2D analysis does not account for the spatial orientation of the sheets with respect to the cutting plane. As demonstrated in [8], this will affect only the tail for large l_d. The left panel of Fig. 3 compares the PDFs for two different

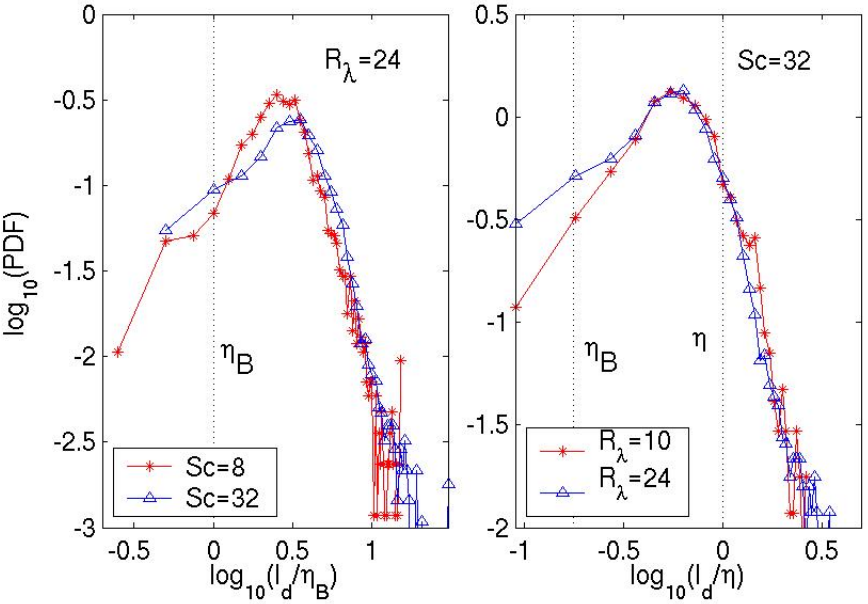

FIG. 3: (color online) Distribution of the local cross-section thickness l_d of the scalar dissipation rate filaments for $\epsilon_\theta \geq 4\langle\epsilon_\theta\rangle$. Left panel: Probability density function (PDF) $p(l_d/\eta_B)$ for two different Schmidt numbers at $R_\lambda = 24$. Right panel: PDF $p(l_d/\eta)$ for two different Reynolds numbers at $Sc = 32$.

Schmidt numbers at a fixed Reynolds number. With increasing Schmidt number stronger jumps of the scalar concentration across finer thickness scales become more probable since diffusion is less dominant. Consequently, the most probable thickness, l_d^*, is shifted to smaller values, but remains always larger than the corresponding Batchelor scale. This suggests that the formation of so-called mature scalar gradient fronts with a thickness $\sim \eta_B$ is a subdominant process. We see that both PDFs overlap when rescaled with η_B which implies that $l_d^* \sim Sc^{-1/2}$. In the right panel of Fig. 3, we compare distributions for two different Reynolds numbers at fixed Schmidt number. Both PDFs rescaled with the corresponding η overlap again to a large fraction, except for the very fine scales. Their higher probability with increasing R_λ indicates a more efficient stirring at the smallest scales. The scale l_d^* follows now the same dependence with Reynolds number as the Kolmogorov scale, i.e. $l_d^* \sim R_\lambda^{-3/2}$, similar to [8, 9] for $Sc \sim 1$. Consequently, the result does not change for $Sc \gg 1$.

Connection to advecting turbulent flow. The filament thickness distributions have to be related now to stretching and contraction processes of the underlying advecting flow. Mostly, the formation of scalar dissipation sheets for $Sc > 1$ has been studied as a reduction of the

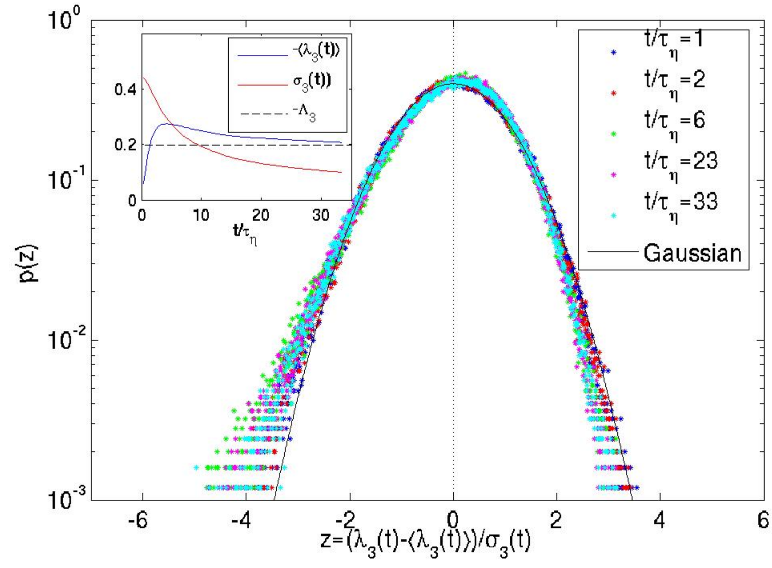

FIG. 4: (color online) Probability density function of the contractive FTLE $\lambda_3(t)$ for different times which are indicated in the legend. The data are for $R_\lambda = 10$. The variable $z = (\lambda_3(t) - \langle\lambda_3(t)\rangle)/\sigma_3(t)$ with $\sigma_3(t) = \sqrt{\langle(\lambda_3(t) - \langle\lambda_3(t)\rangle)^2\rangle}$ is chosen in order to compare it directly with a Gaussian distribution. The inset shows the temporal convergence of $\langle\lambda_3(t)\rangle$ to the asymptotic value Λ_3 (dashed line) and $\sigma_3(t)$. The distribution is evaluated by 2.5×10^5 Lagrangian tracers that are initially seeded uniformly in the simulation box. $\tau_\eta = \sqrt{\nu/\langle\epsilon\rangle}$ is the Kolmogorov time. The distribution for $R_\lambda = 24$ behaves qualitatively the same.

Eulerian dynamics to the direction of contractive strain with a time-dependent rate $\gamma(t) < 0$ [8, 15, 16]. Since the present geometric analysis is statistical, it seems natural to relate it to the statistics of local contraction rates in the flow. The latter are fully determined by the distribution of the three finite-time Lyapunov exponents (FTLE) along separate Lagrangian tracer tracks, $\lambda_i(t)$. They measure the separation between two initially infinitesimally close fluid elements in the Lagrangian framework, given by $|\delta\mathbf{r}|$. This separation vector evolves as $\mathrm{d}\delta r_j(t)/\mathrm{d}t = \sigma_{jk}(t)\,\delta r_k(t)$ for $j,k = x,y,z$, where $\sigma_{jk}(t)$ is the rate of strain tensor along the Lagrangian trajectories. The FTLEs follow from an algorithm by Benettin *et al.* [17] to $\lambda_i(t)$=$1/t\,\log(|\delta\mathbf{r}^{(i)}(t)|/|\delta\mathbf{r}^{(i)}(0)|)$. Their mean over an ensemble of Lagrangian tracers are the global FTLE $\langle\lambda_i(t)\rangle$. They converge for long times to the (asymptotic) Lyapunov exponents $\Lambda_i = lim_{t\to\infty}\langle\lambda_i(t)\rangle$. Due to incompressibility, $\sum_{i=1}^{3}\lambda_i(t) = 0$. Our interest is in the formation of thin dissipation (or gradient) sheets where expansion in two directions is present, i.e. $\lambda_1(t) > 0$ and $\lambda_2(t) > 0$, and contraction in the third one, $\lambda_3(t) < 0$. The distribution of contractive local flows that pile up such maxima follows consequently from the PDF $p(\lambda_3(t))$ which is shown in Fig. 4. We see that the distributions for different times collapse almost perfectly with a Gaussian profile within $\pm 3\sigma_3(t)$. Since the standard deviation $\sigma_3(t)$ is monotonically decreasing with time (see inset of Fig. 4) the contraction rate $\lambda_3(t)$ will get more and more concentrated about Λ_3 as the time progresses.

Based on the Lyapunov exponent Λ_3 the most probable thickness can be calculated as $l_d^* = \sqrt{\kappa/|\Lambda_3|}$ [18] which arises by equilibrating contractive strain and diffusion. For all data analysed this scale is at about the maximum of the thickness distribution. Hu and Pierrehumbert [2] pointed out that Λ_3 is not adequate to explain the formation of largest dissipation amplitudes observed in mixing and that short-time contraction events are necessary to pile up filaments with thickness below l_d^*. In addition, Ref. [11] showed in Eulerian framework that large scalar gradients are found to a significant fraction in the vicinity of local vortical flow topologies, especially for larger Sc. The latter contributions are assigned with more rapid rotations of the δr_i along the Lagragian tracer tracks and are filtered out in a long-time limit. We will therefore take the short-time dependence of the contractive flow motion into account. The decrease of the local thickness scales will follow $l_d(t) = l_0 \exp(\lambda_3(t)t)$. The scale distribution results then to $p(l_d) = \int_{L_-}^{L_+} \mathrm{d}l_0\, p(l_0) \int_{-\infty}^{+\infty} \mathrm{d}\lambda_3\, g(\lambda_3)\, \delta\left(l_d - l_0 \mathrm{e}^{\lambda_3 t}\right)$, where the Gaussian distribution $g(\lambda_3) = (1/\sqrt{2\pi\sigma_3^2}) \exp[-(\lambda_3 - \langle\lambda_3\rangle)^2/(2\sigma_3^2)]$ with the (yet unknown) distribution of the initial thickness scales is combined. The physical picture that we have in mind is that at the beginning of the formation a continuum of scales is already present and that we can take the simplest case, an equipartition between $L_- = \eta_B$ and $L_+ = \eta$. It follows

$$p(l_d) = C \frac{l_d t \exp\left(\frac{\sigma_3^2 t^2}{2} - \langle\lambda_3\rangle t\right)}{2(\eta - \eta_B)} [\mathrm{erf}(X_+) - \mathrm{erf}(X_-)], \tag{3}$$

with $X_\pm = (1/\sqrt{2}\sigma_3)[(1/t)\log(l_d/L_\pm) - \langle\lambda_3\rangle + \sigma_3^2 t]$ and C being a normalization constant. The error function is $\mathrm{erf}(x) = (2/\sqrt{\pi}) \int_0^x \exp(-y^2)\mathrm{d}y$. Figure 5 shows the resulting thickness PDFs that follows from (3) at shorter times t for $R_\lambda = 10$ and $Sc = 32$. We see that they overlap well with the thickness distribution following from the data analysis. With progressing time the distribution seems to fit less well, especially with the smallest scales (see the data at $t/\tau_\eta = 10$ in Fig. 5). The time-dependence confirms that mostly formation processes at a short time scale (here $\sim 2\tau_\eta$) are responsible for the steepening of intensive

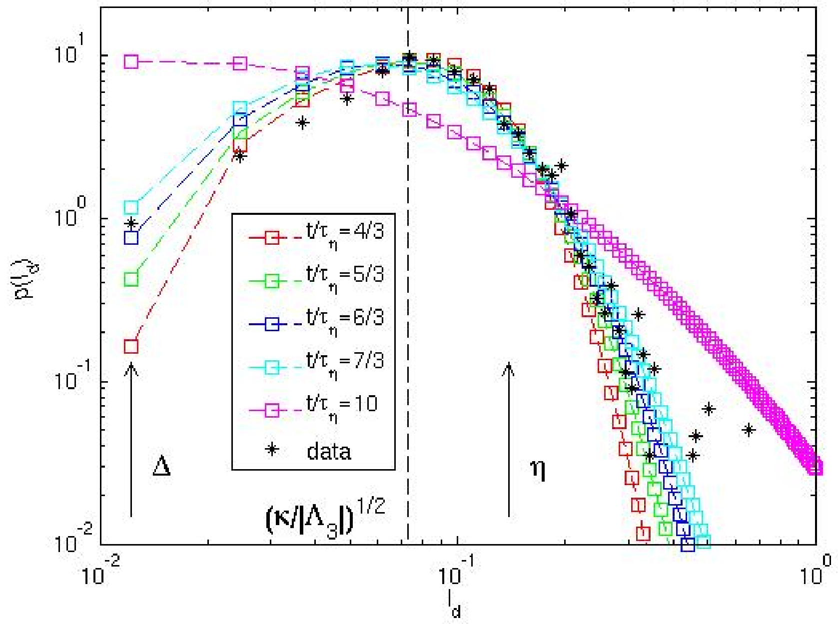

FIG. 5: (color online) Distribution of the local cross-section thickness l_d as reconstructed from $p(\lambda_3(t))$ via Eq. (3) for different times. The black data points are directly evaluated (see the red curve in the right panel of Fig. 3). Data are for $R_\lambda = 10$ and $Sc = 32$. The most probable thickness $l_d^* = \sqrt{\kappa/|\Lambda_3|}$ is indcated as a dashed line, grid spacing Δ and Kolmogorov scale as vertical arrows.

gradient structures. We verified this for all our data sets. To conclude, the distribution of short-time contraction events is able to explain the numerically found distribution of the thickness scales. A potential extension of the present work would be the inclusion of $\lambda_1(t)$ and $\lambda_2(t)$ and to study the lateral extension of the dissipation maxima. This requires a three-dimensional analysis and will be part of future work.

Acknowledgments. We acknowledge support by the NSF grant DMS-9810282 and thank the Institute for Pure and Applied Mathematics at UCLA for hospitality during the Multiscale Geometric Analysis program. J.S. was also supported by the DFG. The simulations were done on the JUMP cluster at the John von Neumann-Institute for Computing at the Forschungszentrum Jülich.

[1] C. Wunsch and R. Ferrari, Annu. Rev. Fluid Mech. **36**, 281 (2004); L. Verwisch and T. Poinsot, Annu. Rev. Fluid Mech. **30**, 655 (1998); D. Rothstein, E. Henry, and J. P. Gollub, Nature

401, 770 (1999).

[2] Y. Hu and R. T. Pierrehumbert, J. Atmos. Sci. **59**, 2830 (2002);

[3] G. K. Batchelor, J. Fluid Mech. **5**, 113 (1959).

[4] J.-L. Thiffeault, C. R. Doering, and J. D. Gibbon, J. Fluid Mech. **521**, 125 (2004); C. R. Doering and J.-L. Thiffeault, preprint physics/0508151 (2005).

[5] *Turbulent combustion* (Cambridge University Press, Cambridge, England, 2000).

[6] T. M. Antonsen, Z. Fan, E. Ott, and E. Garcia-Lopez, Phys. Fluids **8**,3094 (1996).

[7] C. H. Gibson, Phys. Fluids **11**, 2305 (1968).

[8] K. A. Buch and W. J. A. Dahm, J. Fluid Mech. **364**, 1 (1998).

[9] L. K. Su and N. T. Clemens, J. Fluid Mech. **488**, 1 (2003).

[10] B. W. Zeff, D. D. Lanterman, R. McAllister, R. Roy, E. J. Kostelich, and D. P. Lathrop, Nature **421**, 146 (2003); J. A. Mullin and W. J. A. Dahm, Exp. Fluids **38**, 185 (2005).

[11] J. Schumacher and K. R. Sreenivasan, Phys. Rev. Lett. **91**, 174501 (2003); J. Schumacher, K. R. Sreenivasan, and P. K. Yeung, J. Fluid Mech. **531**, 113 (2005).

[12] D. Kushnir, M. Galun, and A. Brandt, Pattern Recognition, in press (2006).

[13] A. Brandt, S. McCormick, and J. Ruge. *Algebraic multigrid (AMG) for automatic multigrid solution with application to geodetic computations.* Inst. for Computational Studies, POB 1852, Fort Collins, Colorado, 1982.

[14] E. Sharon, A. Brandt, and R. Basri, Proc. IEEE Conf. on Computer Vision and Pattern Recognition, Vol. 1, 70 (2000).

[15] G. F. Carrier, F. E. Fendell, and F. E. Marble, SIAM J. Appl. Math. **28**, 463 (1975).

[16] E. Villermaux and J. Duplat, Phys. Rev. Lett. **91**, 184501 (2003).

[17] G. Benettin, L. Galgani, A. Giorgilli, and J.-M. Strelcyn, Meccanica **15**, 21 (1980).

[18] E. Balkovsky and A. Fouxon, Phys. Rev. E **60**, 4164 (1999).